Journal of The Electrochemical Society, **153** (3) A543-A553 (2006)
0013-4651/2006/153(3)/A543/11/$20.00 © The Electrochemical Society

Low Crossover of Methanol and Water Through Thin Membranes in Direct Methanol Fuel Cells

Fuqiang Liu,[a,b] Guoqiang Lu,[b,c] and Chao-Yang Wang[a,b,c,*,z]

[a]*Electrochemical Engine Center,* [b]*Department of Materials Science and Engineering, and* [c]*Department of Mechanical and Nuclear Engineering, The Pennsylvania State University, University Park, Pennsylvania 16802, USA*

Low crossover of both methanol and water through a polymer membrane in a direct methanol fuel cell (DMFC) is essential for using high concentration methanol in portable power applications. A novel design of the membrane-electrolyte assembly (MEA) has been developed in this work to attain low methanol crossover, low water crossover, and high cell performance simultaneously. The anode catalyst layer, in the form of a catalyzed diffusion medium (CDM), serves as a methanol diffusion barrier to reduce methanol crossover. In addition, a highly hydrophobic cathode microporous layer (MPL) is employed to build up the hydraulic pressure at the cathode and hence drive the product water from the cathode into the anode to offset the water dragged by electro-osmosis. The new MEA, consisting of a CDM anode, a thin Nafion membrane, and a carbon cloth precoated with an MPL on the cathode, is shown to attain: (*i*) a net water transport coefficient through the membrane smaller than 0.8 at 60°C and 0.4 at 50°C; (*ii*) fuel efficiency of ~80%; and (*iii*) a steady-state power density of 60 mW/cm^2 at ca. 0.4 V and 60°C with low stoichiometric flow rates of ambient dry air and 3 M methanol solution.
 [DOI: 10.1149/1.2161636]

Manuscript submitted August 24, 2005; revised manuscript received November 8, 2005. Available electronically January 26, 2006.

Direct methanol fuel cells (DMFCs) promise to power future micro- and portable electronic devices owing to their high energy density and inherent simplicity of operation with methanol as the liquid fuel.[1] A vast majority of the research efforts in the literature has been focused on developing new electrocatalysts to improve sluggish methanol oxidation and new electrolyte materials to reduce methanol crossover through the polymer membrane.[2] Progress in DMFC performance has been steady[3-14] and state-of-the-art power densities are as high as 500 mW/cm^2 under optimized operating conditions such as elevated cell temperatures (>100°C) to promote methanol oxidation reaction, high air stoichiometry (>10) to prevent cathode flooding, and dilute methanol solutions to mitigate methanol crossover.[15] Very dilute methanol solution requires that a large amount of water be carried in the fuel tank and thus drastically reduces the energy density of a DMFC system. Highly concentrated methanol solution, including pure methanol, is preferred for portable power applications.

Unfortunately, the ability to use highly concentrated methanol solution in the anode is largely limited by excessive water loss from the anode to cathode experienced in conventional DMFCs under the influences of electro-osmotic drag (EOD) and molecular diffusion through the membrane. The anode reaction of a DMFC requires an equivalent number of water and methanol molecules, but roughly 2.5×6 water molecules must be dragged through a thick membrane such as Nafion 117 towards the cathode, assuming that one methanol molecule is completely oxidized to produce six protons and the EOD coefficient of water is 2.5 per proton transported through the membrane.[16] This then causes 16 water molecules to be lost from the anode for every methanol molecule consumed, which translates to a methanol concentration of only 10% by weight or about 3 M methanol solution. This calculation clearly indicates that water crossover through a thick membrane already limits the maximum methanol concentration to approximately 3 M, let alone any consideration of methanol crossover.

There exists a large amount of water inside the cathode, however. For example, for the consumption of each methanol molecule at the anode, there are 15 water molecules transported from the anode plus 3 water molecules produced by oxygen reduction reaction. Cathode flooding is thus difficult to avoid at low cell temperatures and/or low air stoichiometry required in portable DMFCs.

Minimizing water crossover through a DMFC membrane is therefore an equally important requirement for portable DMFCs besides methanol crossover mitigation. Let us define the net water transport coefficient, α, as the net water flux through the membrane from the anode to cathode normalized by the protonic flux. To illustrate why low-α is key to the deployment of concentrated fuel, consider an ideal membrane that features zero methanol crossover but water crossover characterized by α. Then, the highest concentration of methanol solution in the anode must require that the H_2O to CH_3OH molecular ratio be greater than $(1 + 6\alpha)$. Table I gives the corresponding MeOH molarity for various α-values. It is clear that for $\alpha \approx 3$, as in typical DMFCs based on Nafion 117, the maximum operational MeOH concentration is about 3 M, as explained earlier. Likewise, in order to enable direct use of 10 M methanol fuel, α must be reduced to below ~0.4. Further, when $\alpha = -1/6$, there is no need to add water in the anode feed or pure methanol operation becomes theoretically possible, in which situation the water molecule needed to oxidize one methanol molecule will come from the product water of oxygen reduction reaction on the cathode.

Peled et al.[17,18] demonstrated low-α values by using a polyvinylidene fluoride (PVDF)-based nanoporous proton-conducting membrane, a liquid water barrier layer (LWBL), and pure oxygen at three bars on the cathode. It was claimed that the LWBL must be a hydrophobic layer free of holes larger than 0.5 μm. Based on the theory of liquid water transport in polymer electrolyte fuel cells,[19,20] we have designed a unique MEA structure which utilizes the microporous layer to build up the hydraulic pressure on the cathode side and then uses a thin membrane (i.e., Nafion 112) to promote the water back-flow under this hydraulic pressure difference. Such MEAs, published first by Lim and Wang[3] and their water crossover property characterized later by Lu et al.,[21] exhibit extraordinarily low α and hence are generally termed low-α MEA technology.[21,22]

Table I. Dependence of maximum allowable anode methanol molarity on α at 20°C.

Molarity (M)	H_2O/MeOH molar ratio	α
1	53.31	8.72
2	25.53	4.09
4	11.64	1.77
6	7.01	1.00
8	4.70	0.62
10	3.31	0.39
17	1.02	0.00
25	0.0	−0.17

* Electrochemical Society Active Member.
z E-mail: cxw31@psu.edu

In the present paper, we describe a novel MEA to meet simultaneous requirements of low-α, low methanol crossover, and high power density. Using methanol solution (up to 4 M), we have obtained α values smaller than 0.8 and 0.4 at 60 and 50°C, respectively. Different anode catalyst structures, cathode gas diffusion media, membranes, and operating conditions were explored. At 60°C, a power density of 58.1 mW/cm^2 was achieved at low stoichiometry using ambient air and 3 M methanol solution.

Experimental

MEA development.— Two different electrode configurations, catalyzed diffusion medium (CDM) and catalyst coated membrane (CCM), were employed as the anode catalyst layer, while CCM was used as the cathode catalyst layer. By combining different anode and cathode structures, two types of MEAs were obtained and studied in this work. MEA-A is composed of a CCM anode and a CCM cathode, while MEA-B is made of a CDM anode and a CCM cathode. A 30 wt % wet-proofed carbon paper (Toray TGPH-090, E-TEK) of 0.26 mm thickness was used as a backing layer on the anode side. While different materials, including carbon paper and carbon cloth, were employed as the cathode backing. MPL was fabricated by coating a mixture of polytetrafluoethylene (PTFE) and carbon on the surface of a wet-proofed backing layer. Carbon cloth with MPL was employed at the cathode for most of the cases in this work, while other cathode diffusion media were used as indicated.

Unsupported Pt/Ru black (HiSPEC 6000, Pt:Ru = 1:1 atomic ratio, Alfa Aesar) and Pt/C catalyst (40% Pt/Vulcan XC72; E-TEK) were used as catalysts for anode and cathode, respectively. To make a CDM, a solvent-substituted Nafion solution in Na^+ form,[3,23] prepared from commercial 5 wt % Nafion solution (EW 1100, DuPont), was mixed with Pt/Ru black to form a slurry. The slurry was coated on the MPL of the anode backing to form the anode catalyst layer, followed by heat-treatment and re-protonation. The CCM anode was prepared by a decal method.[21] The catalysts were first wetted by a small amount of DI water, followed by addition of isopropanol, 5 wt % Nafion solution, and ethylene glycol. After sufficient period of magnetic stirring, the mixture ink was treated ultrasonically for 1–2 min and then coated on a Teflon substrate. The coated Teflon film was dried for several hours in an oven at 80°C before being hot-pressed to a pretreated Nafion membrane at 125°C and 100 atm for 3 min. The loadings of the catalyst layer in this paper were 4.8 mg PtRu/cm^2 and 1 mg Pt/cm^2 for anode and cathode, respectively. The ratio of catalyst to ionomer was maintained to be 4:1 (dry weight) for both anode and cathode.

Single cell testing.— Electrochemical performance evaluation was conducted in a 12 cm^2 graphite cell fixture. The flow fields, consisting of machined two-pass serpentine grooves on graphite blocks, were identical for both anode and cathode. A digital pump (Series I digital pump, Laballiance) with flow rate ranging from 0.01 to 10 mL/min was used to deliver methanol solution and control its flow rate. The flow rate of nonpreheated and nonpressured dry air was controlled by a flow rate controller and the cell temperature was controlled by a digital temperature controller. A water trap containing anhydrous calcium sulfate (W.A. Hammond Drierite Co., Ltd) was connected to the exit of the cathode to collect the water contained in the cathode exhaust. A constant current was maintained for ca. 2 h and the water collected from the cathode was used to calculate the net water transport coefficient, α. DMFC quick-scan polarization curves were obtained by an Arbin testing system in a galvanodynamic mode with a scan rate of 10 mA/s.

Electrochemical characterization.— For methanol crossover measurements, 97 mL/min dry N_2, at the same flow rate of dry air corresponding to stoichiometry of 3 at 150 mA/cm^2, was fed into the cathode. Methanol solution of stoichiometry of 1.75 at 150 mA/cm^2 was fed into the anode. When a positive voltage was applied, the limiting current obtained at N_2-fed cathode corresponded to the oxidation current of the total crossover methanol from the anode to cathode at open circuit. During anode polarization measurement, 100 mL/min room-temperature H_2 was fed to the cathode side as a pseudoreference electrode (dynamic hydrogen electrode, DHE), with respect to which the voltage was applied and methanol oxidation current was recorded. Electrochemical impedance spectroscopy (EIS) was conducted using a Solartron 1278 electrochemical interface in conjunction with a Solartron 1260 frequency response analyzer. The working electrode was connected to the cathode, while the reference and counter electrodes were linked to the anode.

Water balance measurement.— The net water flux (in mol/s) transported from the anode to cathode through the membrane can be expressed as

$$N_{\text{trans}H_2O} = \alpha \frac{IA}{F} \quad [1]$$

where α is the net water transport coefficient. It is a combined result of EOD, diffusion, and hydraulic permeation through the membrane. For thick membranes such as Nafion 117, α approaches the EOD coefficient as the other two modes of water transport become negligible. Positive α corresponds to a net water flow from the anode to cathode, while negative α indicates a reserve in the water transport direction.

In the operation of a DMFC, dry air is fed to the cathode, where oxygen is reduced electrochemically via

$$O_2 + 4H^+ + 4e^- \rightarrow 2H_2O \quad [2]$$

The water produced from power generation can thus be described as

$$N_{\text{power}H_2O} = 0.5\frac{IA}{F} \quad [3]$$

where I, A, and F are the current density, electrode area, and Faraday constant, respectively.

The crossover methanol is oxidized at the cathode side following Eq. 4

$$CH_3OH + 1.5\ O_2 \rightarrow CO_2 + 2H_2O \quad [4]$$

Assuming all crossover methanol is oxidized by the positive potential at the cathode, the water produced by methanol oxidation can be calculated from

$$N_{\text{oxi}H_2O} = \frac{1}{3}\frac{I_c A}{F} = \frac{1}{3}\frac{1-\eta_{\text{fuel}}}{\eta_{\text{fuel}}}\frac{IA}{F} \quad [5]$$

where I_c is the methanol crossover current density, and η_{fuel} the fuel efficiency defined as

$$\eta_{\text{fuel}} = \frac{I}{I + I_c} \quad [6]$$

Combining Eq. 1, 3, and 5 yields the total water flow rate at the cathode exhaust

$$N_{H_2O} = 0.5\frac{IA}{F} + \alpha\frac{IA}{F} + \frac{1}{3}\frac{1-\eta_{\text{fuel}}}{\eta_{\text{fuel}}}\frac{IA}{F} \quad [7]$$

Note that the above equation is valid with dry air inlet only. The net water transport coefficient can thus be measured according to

$$\alpha = N_{H_2O}\cdot\frac{F}{IA} - 0.5 - \frac{1}{3}\frac{1-\eta_{\text{fuel}}}{\eta_{\text{fuel}}} \quad [8]$$

The last term in Eq. 8 can be estimated from the fuel efficiency, e.g., it is equal to 0.083 at 80% fuel efficiency. For convenience, we will report α by its apparent value, which includes water produced from the oxidation of crossover methanol, i.e., $(N_{H_2O}F/IA - 0.5)$. The difference between the actual α and its apparent value is equal to $(1-\eta_{\text{fuel}})/(3\eta_{\text{fuel}})$. Note that α-values reported in this paper are higher than the actual net water transport coefficient through the membrane by ~0.1.

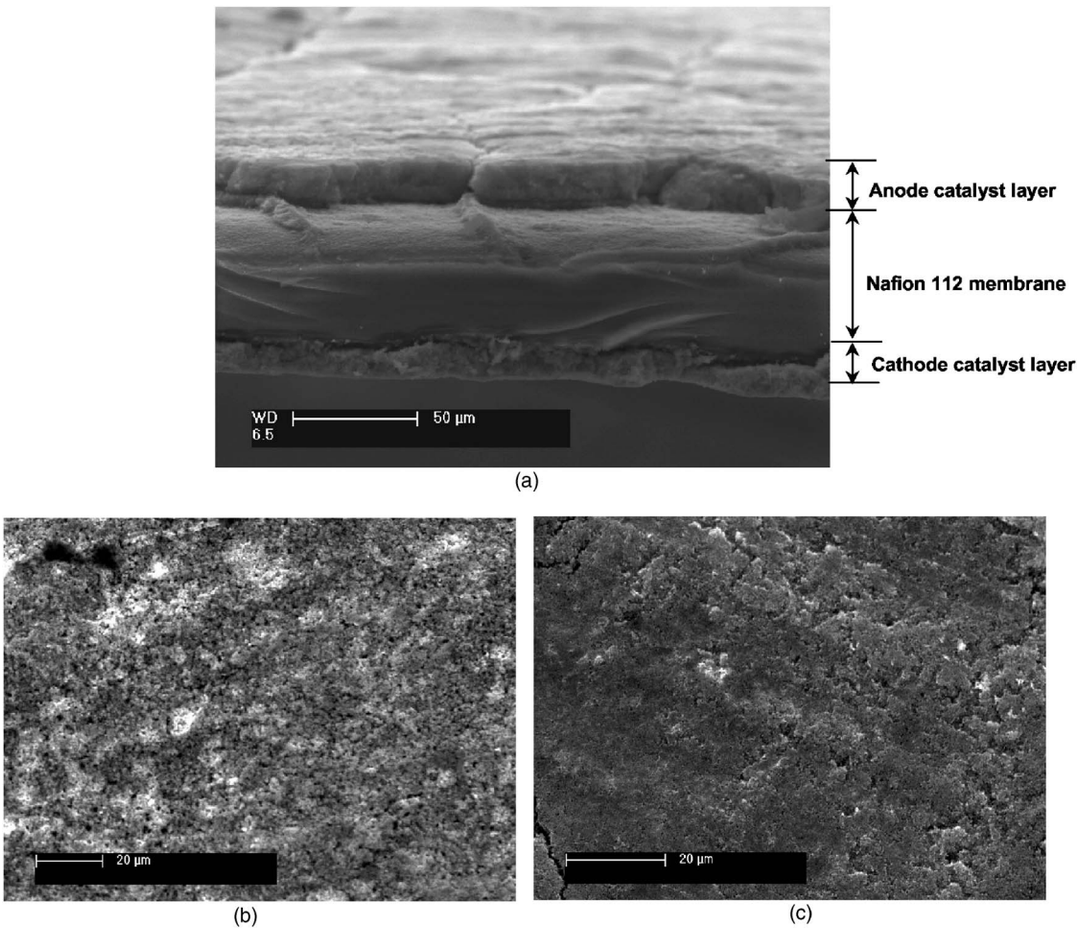

Figure 1. SEM micrographs of MEA-A: (a) cross section; (b) surface of CCM anode catalyst layer; and (c) surface of CCM cathode catalyst layer.

Results and Discussion

Scanning electron micrographs (SEM).— Cross-section and surface morphologies of CCM and CDM catalyst layers are shown in Fig. 1 and 2. The surface of the CCM cathode catalyst layer is very flat with small cracks scattering on it. Its thickness is only ca. 25 μm, as shown in Fig. 1a. High loading (1 mg Pt/cm^2) and very thin cathode catalyst layer ensure good activity and low mass transport resistance. The CDM anode is more porous than the CCM anode, and its catalyst layer forms a bimodal pore distribution with small primary pores in the agglomerates formed by PtRu black and Nafion, and large secondary pores with diameter of ca. 5–10 μm between agglomerates. The catalyst and ionomer are considered to be more closely packed in the CCM anode, and the diameter of secondary pores in the catalyst layer is much smaller, as shown in the SEM picture of Fig. 1b. The thickness of the CCM anode catalyst layer is about 20–30 μm, much thinner than that of CDM, about 50 μm in thickness (Fig. 2a). Because the same PtRu black and Nafion loading were used for the two anode catalyst layers, the thick CDM anode is expected to exhibit higher methanol transport resistance than the CCM anode; hence, it has a lower methanol crossover current density, as is shown below.

Influence of anode catalyst layer.— As shown in the SEM pictures, CDM and CCM anode catalyst layers feature different microstructures; therefore, they may have different methanol and water transport properties. The methanol crossover and anode polarization of the two anode catalyst layers are characterized in Fig. 3a and b. In Fig. 3a, the cell with the CDM anode has a lower methanol crossover current density than the CCM anode, owing to the thicker CDM anode. For example, at 3 M methanol solution, the crossover current density at open circuit in the cell with the CDM anode is 206 mA/cm^2, compared with 227 mA/cm^2 of the cell with the CCM anode. At 2 M methanol solution, the crossover current density in the CDM anode cell declines further to 169 mA/cm^2. Also, different internal structure, the interaction between PtRu catalyst and ionomer, and the catalyst layer thickness of the two anode catalyst layers result in different anode polarization behaviors. With 2 M methanol feed, the CDM anode has a smaller limiting current density, ca. 210 mA/cm^2, compared with 247 mA/cm^2 of the CCM anode, but it outperforms the CCM anode cell at current density below ca. 130 mA/cm^2, indicating that methanol crossover is smaller and there is a more extensive catalyst/ionomer interface forming in the CDM anode catalyst layer. At current densities higher than 130 mA/cm^2, the potential versus DHE in the CDM anode increases dramatically and shows severe mass transport limiting current.

Water transport and cell performance of MEA-A and MEA-B are analyzed under various operating conditions in Fig. 4 and 5, respectively. Note that the only difference of the two MEAs is the anode: MEA-A has a CCM anode while MEA-B has a CDM anode. The anode catalyst layers have no effect on the water crossover coefficient; the net water transport coefficient α is about 0.4 at 50°C and 0.8 at 60°C for the 2 M methanol solution, regardless of which anode configuration is used.

Nonetheless, performance of the cells with two MEAs differs owing to different anodes. As expected, the limiting current densities in quick-scan polarization curves for the CCM anode cell are always

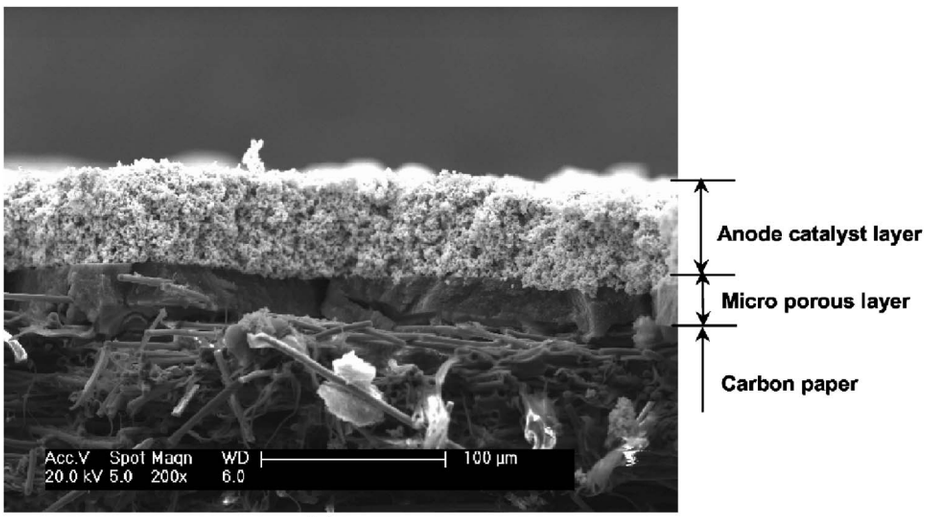

(a)

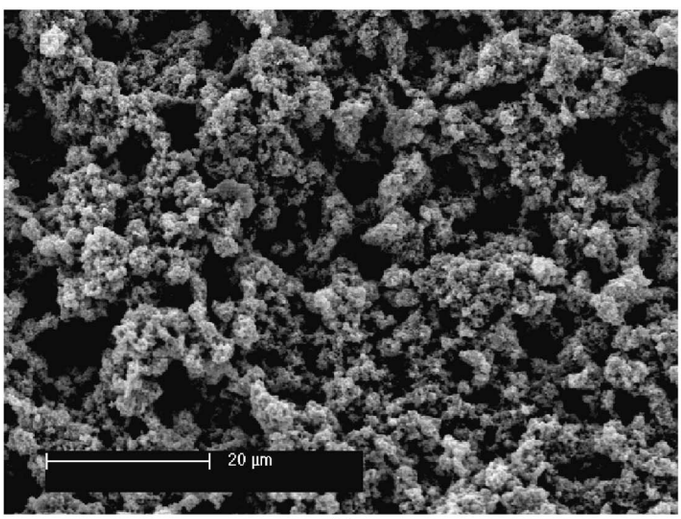

(b)

Figure 2. SEM micrographs of MEA-B: (a) cross section; and (b) surface of CDM anode.

larger than that of the CDM anode cell, and the difference between them is approximately 50 mA/cm^2. For example, at 60°C and anode/cathode stoichiometries of 2/3 at 150 mA/cm^2, the limiting current densities of the CCM anode and CDM anode cells are 264 and 221 mA/cm^2, respectively. The difference between these two MEAs is more significant under steady-state constant current discharge. In Fig. 4a, the cell voltages at 150 mA/cm^2 are almost independent of the anode stoichiometry in the CCM anode cell at 60°C. Even at the difference between average cell voltages for anode stoichiometries of 1.75 and 2.5 is only 15 mV, while the anode stoichiometry has a much larger effect on the CDM anode cell, especially at low cell temperatures. It is seen from Fig. 5a that the average cell voltage at 150 mA/cm^2 in the CDM anode cell is 0.246, 0.290, and 0.309 V for anode stoichiometries of 1.75, 2, and 2.5, respectively. At 50°C the difference between average cell voltages for various anode stoichiometries becomes much larger: 180 mV between stoichiometries of 1.75 and 2.5 at 150 mA/cm^2. In fact, the CDM anode cell cannot operate stably at 50°C and low anode stoichiometry. However, note that the quick-scan polarizations display little dependence on anode stoichiometries. In the Fig. 5b inset, cell voltages are almost identical up to ca. 150 mA/cm^2, and the difference between limiting current densities at different anode stoichiometries is within ca. 10 mA/cm^2.

Anode sthoichiometry is a more critical parameter of performance stability at constant current discharge than in quick-scan polarization, especially for the CDM anode at 50°C. Constant current discharge over an extended period of time requires steady-state or quasi-steady-state operation; that is, the rate of fuel delivery from the anode channels through the backing into the catalyst layer should balance with the rate of fuel consumption in the catalyst layer. Otherwise, cell discharge performance would not be stable. Figure 6 displays performance of a CDM anode cell based on a Nafion 1135 membrane discharged with 3 M methanol solution. It is seen that the cell voltages are very stable and show small variation and decay with time for all anode stoichiometries. The difference between the average voltages at different anode stoichiometries is very small, indicating that diffusion of methanol to the anode catalyst layer is sufficient even at low stoichiometry, which is favored by higher methanol concentration gradient across the anode catalyst layer. A steady-state power density of 58.1 mW/cm^2, obtained by averaging the power densities over the discharge time, was reached with anode/cathode stoichiometry of 2.5/3 at 150 mA/cm^2 using ambient air and 3 M methanol solution. In quick-scan polarization curves (see the inset of Fig. 6), the limiting current density can reach 300 mA/cm^2 for anode stoichiometry of 2.5 at 150 mA/cm^2.

The thicker CDM anode catalyst layer creates a higher resistance

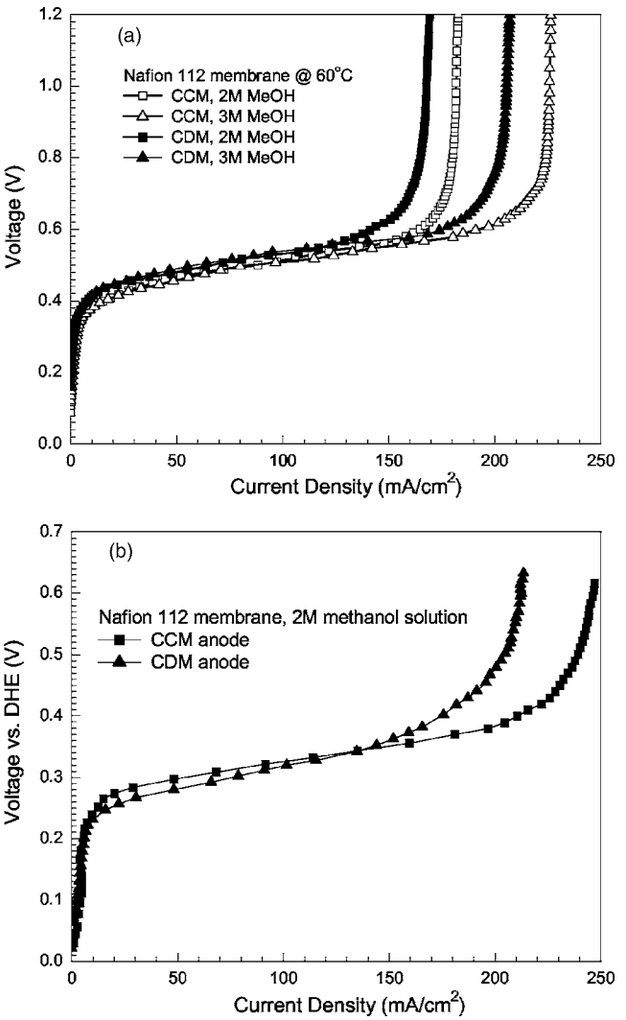

Figure 3. Comparison of CCM and CDM anode catalyst layers: (a) methanol crossover; and (b) anode polarization. Carbon paper and carbon cloth both with MPL were employed as diffusion media in the anode and cathode, respectively. The cell temperature is 60°C. The flow rate of methanol solution corresponds to 1.75 at 150 mA/cm^2.

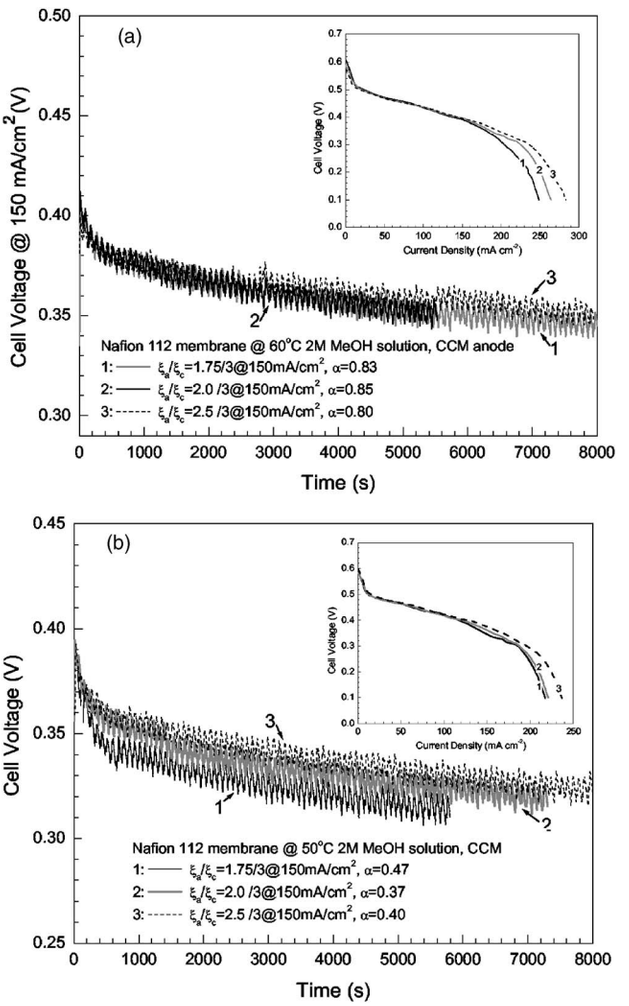

Figure 4. Influence of anode stoichoimetry on constant current discharge in the CCM anode cell using 2 M methanol solution at: (a) 60°C; and (b) 50°C. The insets show quick-scan polarization curves at different anode stoichiometries.

to methanol transport, thereby controlling the rate of methanol reaching the polymer membrane and reducing the crossover current density. Liu et al.[9] pointed out that PtRu black catalysts showed a lower mass transport resistance than carbon-supported PtRu catalysts in the anode catalyst layer for DMFCs. Our results further indicate that the anode catalyst layer properties are highly sensitive to the fabrication procedures; with the same PtRu and Nafion loadings, the CDM anode is more methanol resistant than the CCM anode.

Both the methanol-resistant anode and low-α MEA are useful to achieve the ultimate goal of feeding highly concentrated or pure methanol to DMFCs. A methanol-resistant anode can regulate methanol crossover through the Nafion membrane even in the presence of highly concentrated methanol solution on the anode side, and low-α ensures the water loss from the anode will always be less than the small amount of water supply available from a high concentration methanol solution. Tailoring the anode catalyst layer is thus an important means to realize both goals simultaneously. A thicker and denser anode catalyst layer can substantially mitigate methanol crossover through the membrane, while affecting water crossover through the membrane only insignificantly. More work is underway to optimize the anode catalyst layer for further simultaneous reduction in both methanol and water crossover.

Membrane thickness effect.— Methanol and water transport through the cell can be enhanced or retarded by membrane thickness. Figure 7 summarizes methanol crossover current densities of Nafion 112 and 1135 membranes at 60°C using different methanol concentrations. It is seen that the crossover current density is approximately linearly proportional to the methanol concentration, with the Nafion 112 membrane featuring higher crossover rate, as expected. The difference in crossover current density between the two membranes diminishes with methanol concentration; for example, the difference decreases from 32 mA/cm^2 at 2 M to 11 mA/cm^2 at 4 M.

The cell resistance, net water transport coefficient, and power density for Nafion membranes of differing thickness are given in Table II for 60°C and 3 M methanol solution. Thicker membranes have higher cell internal resistance, but lower methanol crossover. Therefore, the cell using Nafion 1135 has the best electrochemical performance, and its power density is insensitive to the anode stoichiometry. Further, it is seen from Table II that the net water transport coefficient, α, is nearly independent of the anode stoichiometry. Note that the thinner membranes appear to have only slightly smaller-α value than the thicker one, although the resistance of wa-

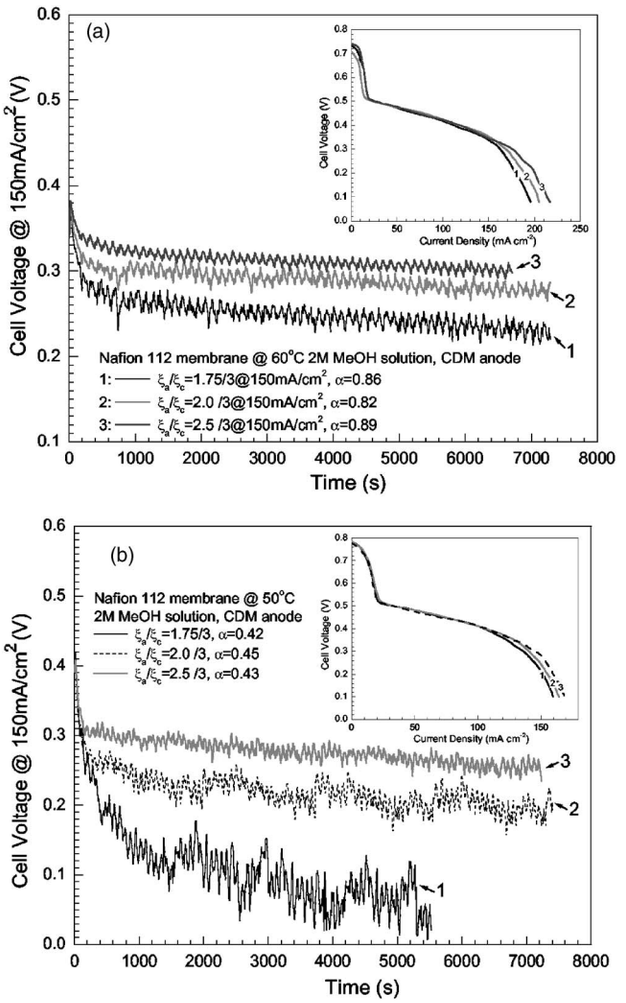

Figure 5. Influence of anode stoichoimetry on constant current discharge in the CDM anode cell using 2 M methanol solution at: (a) 60°C; and (b) 50°C. The insets show quick-scan polarization curves at different anode stoichiometries.

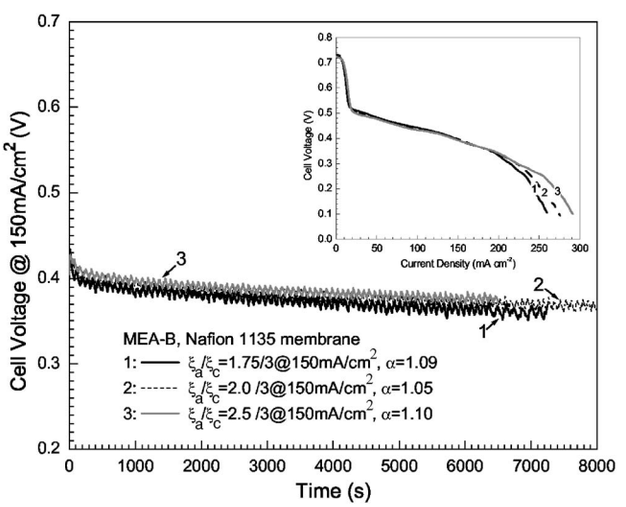

Figure 6. Constant current discharge performance of the CDM anode cell with Nafion 1135 membrane under various anode stoichiometric flow ratios (3 M, 60°C).

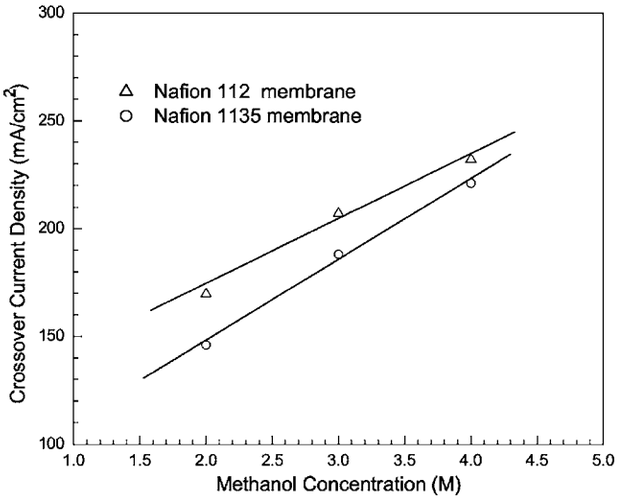

Figure 7. Comparison of methanol crossover current density of Nafion 112 and 1135 membranes at 60°C and different methanol concentrations. MEA-B was used with carbon paper and carbon cloth, both with MPL, as diffusion media in the anode and cathode, respectively.

ter back-flow from the cathode to anode via hydraulic permeation is much reduced in thinner membranes. The net water transport coefficients are 0.70, 0.87, and 1.10 for Nafion 111, 112, and 1135 membranes, respectively, at the stoichiometry (A/C) of 2.5/3. The effect of membrane thickness on water crossover may have been underestimated here because our reported α-value includes water produced from oxidation of methanol crossover. Under common conditions, this is a reasonable assumption because the correction in α would be only about ~0.1, as discussed earlier. However, thinner membranes may have resulted in large methanol crossover current density, I_c, and hence much lower fuel efficiency than 80% used in the estimate of correction. Therefore, the actual water crossover rate through thinner membranes should be smaller than the α-values reported in Table II.

Methanol concentration and anode/cathode stoichiometry effects.— As indicated earlier, methanol diffusion to the anode catalyst layer could be hindered at a low methanol concentration; therefore, part of the catalytic sites cannot be accessed by reactants. A high concentration causes large methanol crossover. Figure 8 shows the steady-state power density and net water transport coefficient at 60°C for various methanol concentrations and anode stoichiometries. The highest steady-state power density is achieved with 3 M methanol solution, as a compromise. For example, at anode/cathode stoichiometries of 1.75/3, the power density in 150 mA/cm^2 discharge increases dramatically from

Table II. Net water transport coefficient, average steady-state power density and cell internal resistance of various membranes.[a]

Membranes		Net water transport coefficient/ Steady-state powder density (mW/cm^2) Nafion 111	Nafion 112	Nafion 1135
Stoichiometries @	1.75/3.0	0.65/19.5	0.64/44.6	1.09/56.4
150 mA/cm^2 (ξ_a/ξ_c)	2.0/3.0	0.61/25.2	0.83/47.1	1.05/57.3
	2.5/3.0	0.70/32.5	0.87/48.6	1.10/58.1
Internal resistance (mΩ cm^2)		135	208	220

[a] MEA-B was used at 3 M methanol solution and 60°C, where both anode and cathode catalyst layers are CDM type, with carbon paper and wet-proofed carbon cloth with precoated MPL as anode and cathode backing layers, respectively.

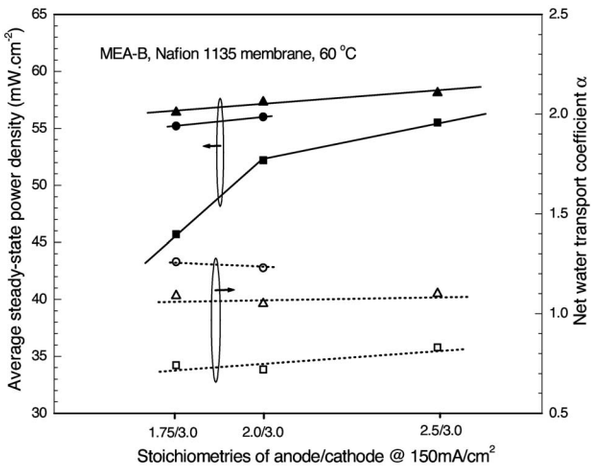

Figure 8. Influence of anode stoichiometry and methanol concentration on average steady-state power density and net water transport coefficient, α. Squares, 2 M methanol solution; triangles, 3 M methanol solution; circles, 4 M methanol solution.

45.7 mW/cm^2 at 2 M to 56.4 mW/cm^2 at 3 M. However, when the concentration is further increased to 4 M, the power density drops to 55.2 mW/cm^2. The steady-state power density increases more noticeably with anode stoichiometry for 2 M methanol solution than 3 and 4 M. For 2 M methanol solution, when anode stoichiometry varies from 1.75 to 2, the power density increases markedly from 45.7 to 52.2 mW/cm^2; and the power density slowly reaches 55.5 mW/cm^2 when the anode stoichiometry further increases to 2.5. For 3 M and 4 M methanol solutions, only slight increase in power density is observed with an increase in the anode stoichiometry.

Although anode stoichiometry and methanol concentration have a large impact on cell performance, they have different influences on water transport; the α value is almost independent of anode stoichiometry, as shown in Fig. 8. On the contrary, methanol concentration seems to have a large impact on α value, i.e., highly concentrated methanol solution results in high α. This trend could be misleading, again, because our reported α value includes water produced from oxidation of crossover methanol. With high methanol solutions, the error of neglecting the methanol crossover effect in estimating α could be gross. For instance, when fuel efficiency decreases to 50 and 40%, respectively, the error becomes 0.333 and 0.5, or greater than 30–50%.

Table III. Effects of operating current density on water crossover coefficient and steady-state power density at 60°C.[a]

Current density (mA/cm^2)	Net water transport coefficient, α	Average steady-state power density (mW/cm^2)
100	1.40	40.8
150	0.85	54.6
200	0.53	61.4

[a] MEA-A, carbon cloth w/ MPL as cathode diffusion media, Nafion 112 membrane, 97 ml/min dry air and 0.19 ml/min 2 M MeOH solution.

The cathode stoichiometry effect on the net water transport coefficient and cell performance is also studied in Fig. 9. As can be seen, the air flow rate has small influence on steady-state and quick-scan performance, indicating that either cathode flooding is not severe or the cathode can still perform reasonably even under partial flooding. However, the net water transport coefficient α has a strong dependence on cathode stoichiometry, increasing from 0.74 to 0.99

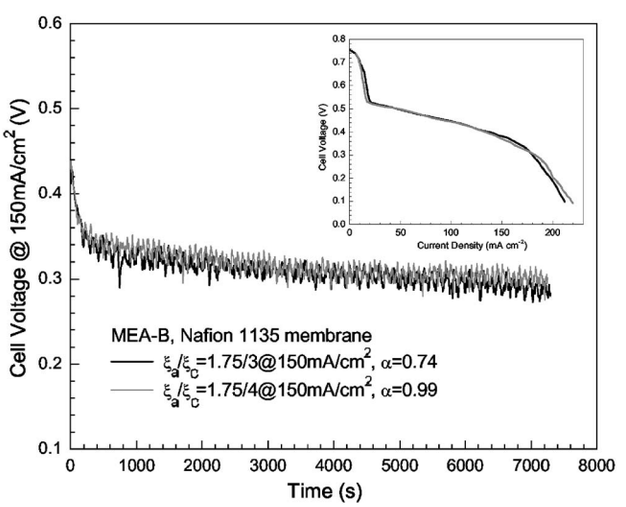

Figure 9. Cathode stoichiometry effect in the CDM anode cell on constant current discharge, net water transport coefficient, and quick-scan performance at 60°C and 2 M.

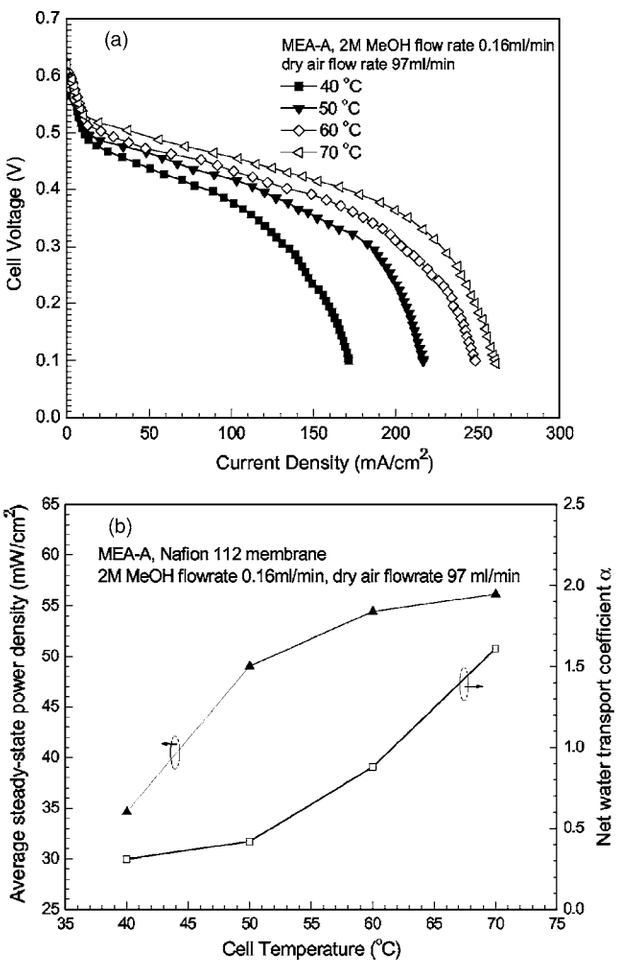

Figure 10. Temperature effects on: (a) quick-scan polarization; and (b) average steady-state power density and net water transport coefficient in constant current discharge. In (b) the operation current density at 40°C is 100 mA/cm^2, while it is 150 mA/cm^2 at 50, 60, and 70°C.

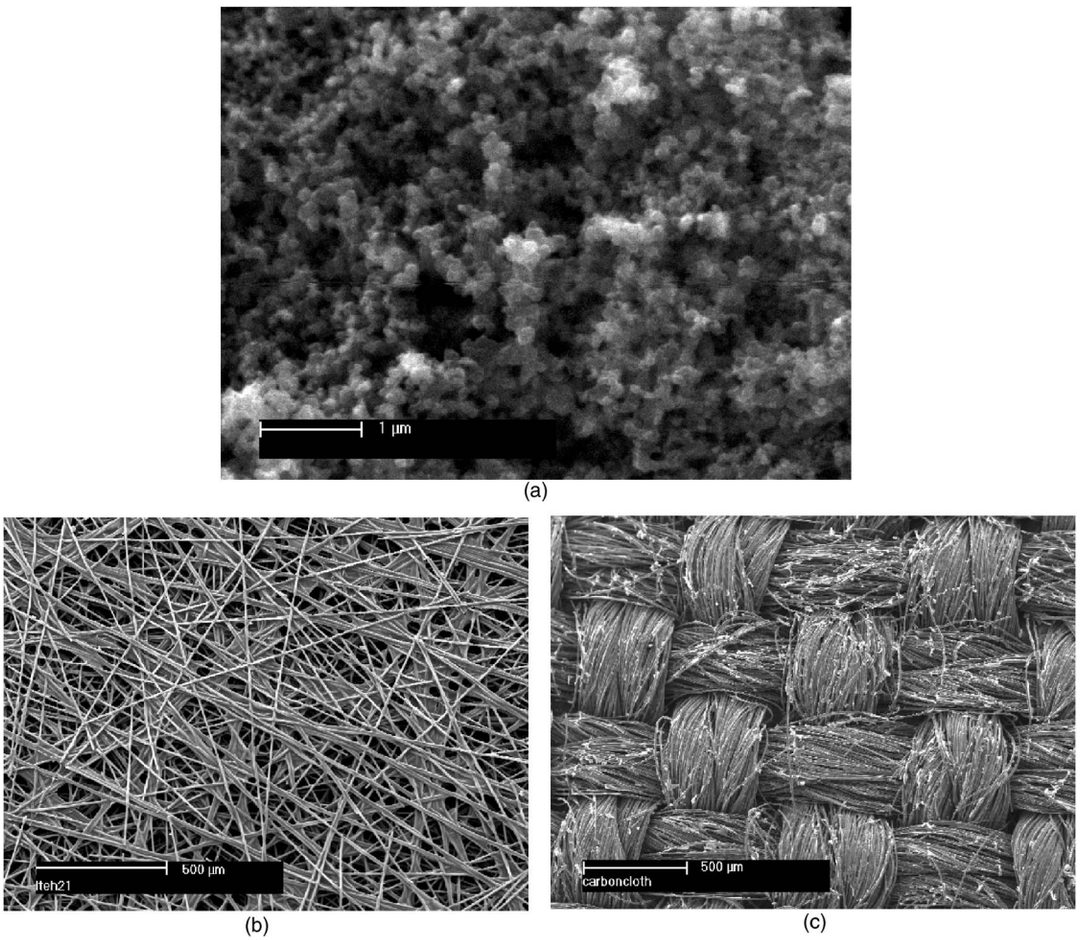

Figure 11. SEM graphs of gas diffusion media: (a) surface of micro porous layer (MPL); (b) wet-proofed carbon paper; and (c) wet-proofed carbon cloth.

when the air stoichiometry varies from 3 to 4. This can be simply explained by the enhanced water evaporation under higher cathode stoichiometry.

Current density and temperature effects.— Water transport through the membrane can be influenced by the operating current density and cell temperature. The water flux to the cathode by diffusion, electro-osmosis, and hydraulic permeation can be expressed as[21]

$$N_{\text{trans}H_2O} = -DA\frac{\Delta c_{c-a}}{\delta_m} + n_d\frac{IA}{F} - \frac{K}{\mu_l}A\Delta p_{c-a}\frac{\rho}{M_{H_2O}} \qquad [9]$$

where ρ is the molar water density, δ_m the membrane thickness, K the hydraulic permeability, n_d the EOD coefficient, μ_l the liquid water viscosity, D the diffusion coefficient, M_{H_2O} the molecular weight of water, Δc_{c-a} and Δp_{c-a} the water concentration difference and the hydraulic pressure difference across the membrane, respectively. Combining Eq. 1 and 9, α can be described as

$$\alpha = -\frac{FD}{I}\frac{\Delta c_{c-a}}{\delta_m} + n_d - \frac{F}{I}\frac{K}{\mu_l}\Delta p_{c-a}\frac{\rho}{M_{H_2O}} \qquad [10]$$

According to Eq. 10, one would expect an increase of α value with current density if both Δc_{c-a} and Δp_{c-a} are constants. However, the experimental results indicate an opposite trend as shown in Table III. Even after correcting the water produced from oxidation of crossover methanol, the net water transport coefficient through the membrane declines from 1.09 at 100 mA/cm^2 to 0.71, and 0.47 at 150 and 200 mA/cm^2, respectively. This clearly indicates that both Δc_{c-a} and Δp_{c-a} are current-dependent variables, and indeed they increase dramatically with the current as the cathode accumulates more water and the anode becomes more gaseous. Both consequences provide a driving force to promote water back-transport from the cathode to anode.

To investigate the effect of temperature on cell performance and water transport, a series of quick-scan polarization curves and net water transport coefficient were measured at different temperatures, and the results are shown in Fig. 10a and b, respectively. The well-defined limiting current densities shown in Fig. 10a are caused by starvation of methanol at the anode side, as confirmed by experiments with increased anode stoichiometry (not shown here). Low methanol flow rate not only reduces the pumping power in a portable application but also lowers methanol crossover through the membrane. In Fig. 10b, the average power density from constant current discharge increases with temperature, as expected. It increases rapidly from 34.6 mW/cm^2 at 40°C to 49.0 mW/cm^2 at 50°C, and levels off when temperature is further increased to 60°C and finally reaches 56.1 mW/cm^2 at 70°C. The net water transport coefficient also increases with temperature, but the trend is contrary to the power density, increasing slowly initially but markedly when the temperature is raised from 60 to 70°C. At 70°C, α becomes 1.61, almost doubling that at 60°C.

It seems that 50–60°C is the optimal temperature range for portable applications. Operating temperature above 70°C is undesirable due to excessive water loss from the cathode exhaust, and temperature below 50°C does not yield high power density.

Influence of cathode gas diffusion media.— Figure 11a-c dis-

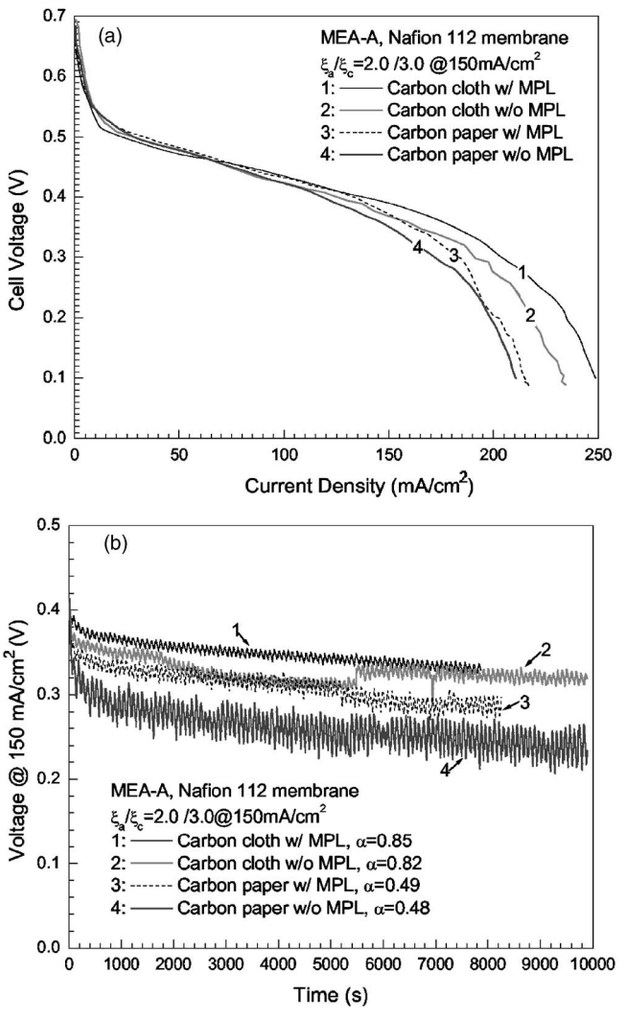

Figure 12. Influence of cathode gas diffusion media on cell performance and net water transport coefficient for MEA-A using 2 M methanol solution at 60°C: (a) quick-scan polarization, and (b) constant current discharge at 150 mA/cm^2.

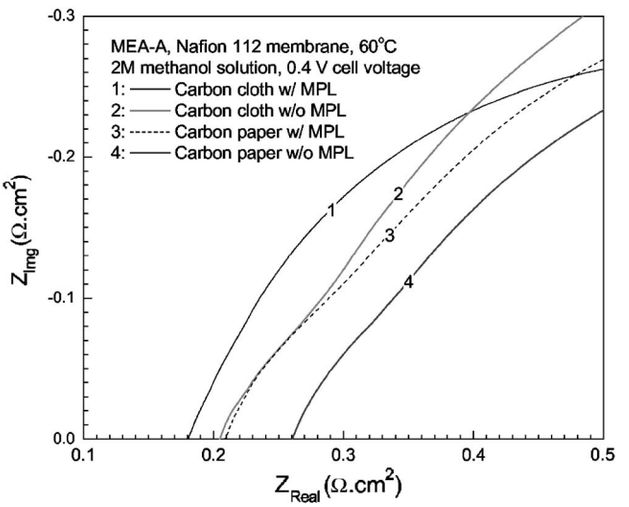

Figure 13. High-frequency portion of EIS spectra of DMFCs using different cathode diffusion media. Anode and cathode stiochiometries are 2 and 3 at 150 mA/cm^2.

plays SEM images of the surfaces of MPL, carbon-paper, and carbon-cloth backings. Carbon paper is a microscopically complex fibrous structure with pore size distribution ranging from a few μm to tens of μm and with a large fraction of blocked passages. Carbon cloth is a woven structure and is generally coarser than carbon paper. Differences in porosity, permeability, pore size distribution, surface wettability, and liquid retention of the two diffusion media result in different two-phase flow and transport characteristics. The MPL is a highly hydrophobic porous structure with pore size much smaller than a backing layer. The combination of high hydrophobicity and small pore size of an MPL creates a substantial liquid pressure on the cathode, which drives liquid water back to the anode side, thus leading to a low net water flux through the membrane. This subsection explores the roles of various backing layers and MPL on the cathode side in affecting the power density and water crossover coefficient. Four cathode diffusion media were tested: carbon paper with and without MPL, and carbon cloth with and without MPL.

Figure 12a and b shows the quick-scan polarization curves and constant current discharge curves of the cells with different cathode gas diffusion media. Carbon cloth with MPL shows the best performance, and carbon paper without MPL the worst. The variation in performance with different diffusion media results primarily from the cell internal resistance as well as the ability of a diffusion medium to facilitate oxygen transport. The cell internal resistance was taken from EIS spectra intercept with real axis as shown in Fig. 13. The internal resistances of carbon cloth with MPL, carbon paper with MPL, carbon cloth without MPL and carbon paper without MPL are 0.181, 0.209, 0.205, and 0.261 Ω cm^2, respectively. It is clear that the presence of MPL improves the electric contact between the catalyst layer and backing layer, thereby resulting in smaller internal resistance, but the difference in internal resistance is responsible for only 12 mV voltage gain at 150 mA/cm^2, much smaller than the 40 mV seen in the quick-scan polarization curves in Fig. 12a or nearly 100 mV exhibited in the constant current discharge. These results show that the dominant effect of carbon cloth backing and MPL is clearly their ability to remove liquid water and thus avoid severe flooding in the cathode catalyst layer. In contrast, carbon paper is more susceptible to cathode flooding.

Surprisingly, we note from Fig. 12b that carbon paper backings have smaller α values than carbon cloth, and α does not change much with the addition of an MPL. The latter observation can be explained by the capillary flow theory of Pasaogullari and Wang.[19] Under steady-state operation, the liquid pressure in a hydrophobic medium is given by capillary pressure expressed as[20,24]

$$p_l = \sigma \cos \theta_c \left(\frac{\varepsilon}{K}\right)^{1/2} J(s) \qquad [11]$$

where ε is the porosity, θ_c contact angle, σ surface tension, and $J(s)$ is the Leverett function of liquid saturation, i.e., the volume fraction of liquid within open pores. The term $(K/\varepsilon)^{1/2}$ is characteristic of the pore size. A schematic illustration of Eq. 11 for MPL and backing layer is given in Fig. 14. Because the MPL pore size is an order of magnitude smaller than that of carbon paper backing layer and the contact angle in MPL is higher, the liquid pressure can be greatly increased by the presence of an MPL under the same liquid saturation, as shown in Fig. 14. If backing layers with MPL and without MPL achieve a similar α due to a similar hydraulic pressure differential across the membrane, the liquid saturation level in the backing layer without MPL must be much higher than that with MPL, as can be seen from Fig. 14. Therefore, the performance of the backing layer without MPL will suffer greatly from cathode flooding. This is consistent with the observation shown in Fig. 12 during constant current discharge. The present explanation can be further verified by the experiments shown in Fig. 15a, in which the air stoichiometry was increased in the cell using carbon paper backing layer without

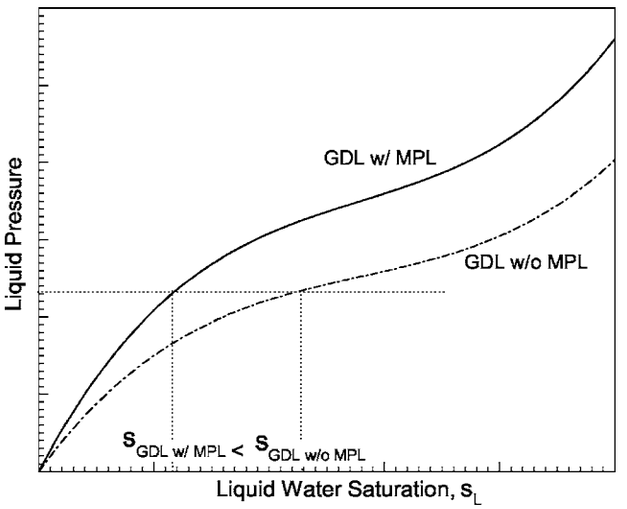

Figure 14. Schematic illustration of liquid pressure as a function of liquid water saturation for backing layers with and without MPL.

MPL. As expected, the degree of cathode flooding is reduced to a level similar to that with MPL, thus producing a comparable or slightly better performance than that with MPL. However, the decreasing liquid saturation in the backing without MPL under large air stoichiometry also reduces the liquid pressure on the cathode, thus leading to higher water crossover from the anode to cathode (shown in Fig. 15b), an undesirable effect from the viewpoint of water management.

Conclusions

Low water crossover, low methanol crossover, and high power density are essential requirements of a direct methanol fuel cell for portable application. In this paper we have described a new MEA design intended to achieve all three goals simultaneously. Specifically, we use a thick and dense CDM anode as a methanol diffusion barrier to mitigate methanol crossover. This approach of limiting methanol crossover through the anode differs from use of thick membranes or development of new membrane materials. Second, an MPL is coated on the cathode backing layer to build up the hydraulic pressure, enabling water back-flow from the cathode to anode. This, in conjunction with a thin polymer membrane, results in 3–4 times lower water crossover coefficient between the anode and cathode. The resulting low-α MEA provides a basic element for future DMFC systems using high concentration or pure methanol. In addition to achieving low crossover of methanol and water, we have demonstrated steady-state power density of $\sim$60 mW/cm^2 at 60°C and $\sim$0.4 V at constant current discharge over several hours.

Extensive parametric studies have been performed to elucidate the effects of material properties, MEA fabrication processes, and operating conditions. Important material properties are the membrane thickness, cathode gas diffusion media, and the microporous layer. It is also found that a CDM anode is more methanol resistant than a CCM anode. Finally, the key parameters of operating conditions include the anode stoichiometry (primarily affecting the methanol crossover), cathode stoichiometry (significantly affecting the water crossover), cell temperature, and current density (both influencing water crossover and power density). A suitable operating range in DMFCs for portable application is found to be between 50 and 60°C, in which high power density ($\sim$60 mW/cm^2) is attainable while crossover of water and methanol can be controlled within an acceptable level.

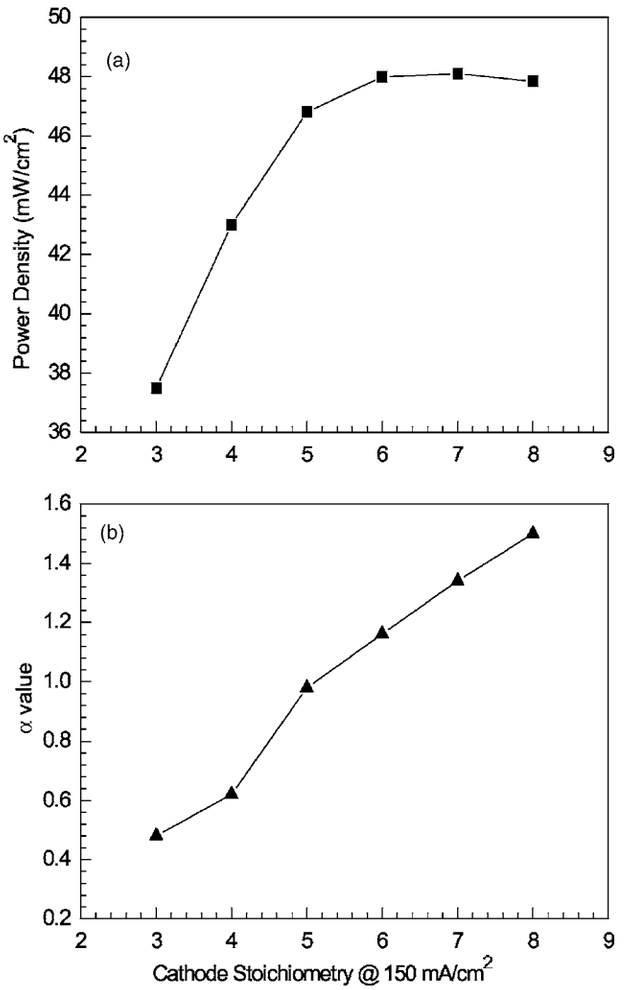

Figure 15. Influence of cathode stoichoimetry on: (a) average power density; and (b) net water transport coefficient in constant current discharge of MEA-A with carbon paper without MPL on the cathode. Anode stoichiometry is 2 at 150 mA/cm^2, and 2 M methanol solution is used at 60°C.

Acknowledgments

This work was supported by DARPA Microsystem Technology Office (MTO) under contract no. DAAH01-1-R001 and by industrial sponsors of ECEC.

The Pennsylvania State University assisted in meeting the publication costs of this article.

References

1. A. S. Aricó, S. Srinivasan, and V. Antonucci, *Fuel Cells*, **1**, 133 (2001).
2. M. A. Hickner, H. Ghassemi, Y. S. Kim, B. R. Einsla, and J. E. McGrath, *Chem. Rev. (Washington, D.C.)*, **104**, 4587 (2004).
3. C. Lim and C. Y. Wang, *J. Power Sources*, **113**, 145 (2003).
4. X. Ren, P. Zelenay, S. Thomas, J. Davey, and S. Gottesfeld, *J. Power Sources*, **86**, 111 (2000).
5. X. Ren, M. S. Wilson, and S. Gottesfeld, *J. Electrochem. Soc.*, **143**, L12 (1996).
6. K. Scott, W. M. Taama, S. Kramer, P. Argyropoulos, and K. Sundmacher, *Electrochim. Acta*, **45**, 945 (1999).
7. G. Halpert, S. R. Narayanan, T. Valdez, W. Chun, H. Frank, A. Kindler, S. Surampudi, J. Kosek, C. Cropley, and A. LaConti, in *Proceedings of the 32nd Intersociety Energy Conversion Engineering Conference*, Vol. 2, p. 774, AIChE, New York (1997).
8. M. Baldauf and W. Preidel, *J. Power Sources*, **84**, 161 (1999).
9. L. Liu, C. Pu, R. Viswanathan, Q. Fan, R. Liu, and E. S. Smotkin, *Electrochim. Acta*, **43**, 3657 (1998).
10. A. S. Aricó, P. Cretì, E. Modica, G. Monforte, V. Baglio, and V. Antonucci, *Electrochim. Acta*, **45**, 4319 (2000).
11. A. S. Aricó, V. Baglio, E. Modica, A. D. Blasi, and V. Antonucci, *Electrochem.*

Commun., **5**, 164 (2004).
12. A. S. Aricó, V. Baglio, A. D. Blasi, E. Modica, P. L. Antonucci, and V. Antonucci, *J. Electroanal. Chem.*, **557**, 167 (2003).
13. A. Heinzel and V. M. Barragan, *J. Power Sources*, **84**, 70 (1999).
14. X. Ren, T. E. Springer, T. A. Zawodzinski, and S. Gottesfeld, *J. Electrochem. Soc.*, **147**, 466 (2000).
15. E. Peled, V. Livshits, M. Rakhman, A. Aharon, T. Duvdevani, M. Philosoph, and T. Feiglin, *Electrochem. Solid-State Lett.*, **7**, A507 (2004).
16. X. Ren and S. Gottesfeld, *J. Electrochem. Soc.*, **148**, A87 (2001).
17. A. Blum, T. Duvdevani, M. Philosoph, N. Rudoy, and E. Peled, *J. Power Sources*, **117**, 22 (2003).
18. E. Peled, A. Blum, A. Aharon, M. Philosoph, and Y. Lavi, *Electrochem. Solid-State Lett.*, **6**, A268 (2003).
19. U. Pasaogullari and C. Y. Wang, *J. Electrochem. Soc.*, **151**, A399 (2004).
20. U. Pasaogullari and C. Y. Wang, *Electrochim. Acta*, **49**, 4359 (2004).
21. G. Q. Lu, F. Q. Liu, and C. Y. Wang, *Electrochem. Solid-State Lett.*, **8**, A1 (2005).
22. G. Q. Lu and C. Y. Wang, in *Transport Phenomena in Fuel Cells*, B. Sunden and M. Fahgri, Editors, WIT Press, Billerica, MA (2004).
23. F. Q. Liu and C. Y. Wang, *Electrochim. Acta*, **50**, 1413 (2005).
24. C. Y. Wang, in *Handbook of Fuel Cells—Fundamentals, Technology and Applications*, W. Lietsich, A. Lamm, and H. A. Gasteiger, Editors, Vol. 3, Part, 3, p. 337, John Wiley & Sons, Chichester (2003).